PHILOSOPHICAL TRANSACTIONS OF THE ROYAL SOCIETY A MATHEMATICAL, PHYSICAL & ENGINEERING SCIENCES

Scanning Electron Acoustic Microscopy and its Applications [and Discussion]

D. G. Davies, R. E. Green, M. Somekh and G. Busse

Phil. Trans. R. Soc. Lond. A 1986 **320**, 243-255
doi: 10.1098/rsta.1986.0114

Phil. Trans. R. Soc. Lond. A **320**, 243–255 (1986)
Printed in Great Britain

Scanning electron acoustic microscopy and its applications

By D. G. Davies
Cavendish Laboratory, Madingley Road, Cambridge CB3 0HE, U.K.

[Plates 1 and 2]

Scanning electron acoustic microscopy (SEAM) is a relatively new technique for imaging and characterization of thermal and elastic property variations on the scale of a few micrometres. A megahertz-chopped, focused electron beam in a scanning electron microscope (SEM) generates sound waves in the sample, and the signal from a transducer attached to the specimen is used to form a scanned image in parallel with the normal SEM image. Although the acoustic wavelengths are typically several millimetres, lateral and depth resolution may be only a few micrometres. This is because image contrast is mainly derived from the micrometre-sized acoustic generation volume just under the beam. In this generation volume, both elastic variations and thermal scattering of the critically damped 'thermal waves', with wavelength of a few micrometres (due to the periodic beam heating), may lead to contrast. There is also evidence for non-thermoelastic contrast generation mechanisms, and these show finer resolution. SEAM shows both advantages and drawbacks compared to conventional scanning acoustic microscopy (SAM). Although understanding of the detailed contrast mechanisms in SEAM is at present only at a qualitative level, it is clear that they are generally different from those in SAM.

The technique is now beginning to attract commercial attention, and applications include imaging of cracks and voids, grains and grain boundaries and second phases in polycrystalline materials, regions of plastic deformation, and magnetic domain structures. Images can be obtained from ICs and semiconductor materials which show doped and implanted regions, near-surface manufacturing defects, and even individual dislocations. The acoustic waves excite vibrational patterns in the specimen, and these can be used as low-resolution probes of, for example, bonding integrity.

1. Introduction

Scanning electron acoustic microscopy (SEAM) represents a new imaging mode on the scanning electron microscope (SEM) (Cargill 1980*a*; Brandis & Rosencwaig 1980) that yields thermal and elastic information typically on the scale of a few micrometres. Chopping of the electron beam causes acoustic waves to be generated in the specimen because of the pulsed energy deposition, and the acoustic signal is used to form a scanned image via a transducer and phase-locked amplifier system. The technique is relatively cheap and simple to implement on an SEM.

Although image contrast is still not completely understood it is clear that an important mechanism is local periodic thermoelastic expansion of the region cyclically heated by the pulsed, focused electron beam. The size of this region depends mainly on the chopping frequency and the thermal conductivity of the material, and at frequencies in the range 10^5–10^6 Hz it extends for about 0.5–10 μm around the electron stopping volume. Spatial variations in thermoelastic and also purely elastic properties and boundary conditions within

and close to this heated volume give rise to image contrast with consequently micrometre-scale lateral and depth resolution. This can be used to image surface-breaking or near-surface cracks, multiple crystalline phases, grain boundaries, plastic deformation and material inhomogeneities. Nonlinear effects (§4*f*) in some materials lead to enhanced resolution, and enable the examination of magnetic domain structures and of phase transformations, which repeat cyclically with the beam modulation.

The acoustic waves have wavelengths of several millimetres, and so act mainly as carriers of the information from the small generation volume. However, their reverberation within the specimen generates vibrational patterns (§4*e*) which can be used as low-resolution acoustic probes of mechanical bonding at large depths.

The technique also seems to be useful in the examination of certain types of semiconductor specimens (§4*b*) and, with some improvements in resolution, it may prove to be an appropriate evaluational tool for the semiconductor industry in particular.

2. Experimental details

In addition to a normal SEM, the apparatus consists of three main components (see figure 1): the beam chopping system, the specimen–transducer assembly, and the amplifier system.

The chopping system applies a unipolar square wave of several volts or tens of volts amplitude to a pair of deflector plates (dimensions approximately 1 cm × 1 cm and separation 1 mm) straddling the beam path. Menzel & Kubalek (1979) give a good discussion of the optimization of such chopping systems.

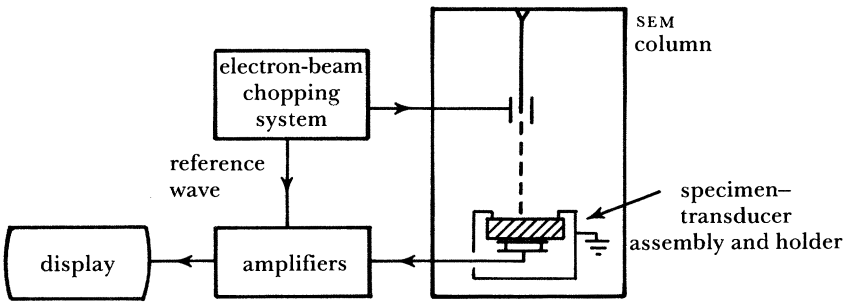

Figure 1. Schematic of an electron–acoustic system.

A solid state transducer (usually 'PZT5') disc in contact with the specimen is used. Good electrical shielding and mechanical contact are ensured by clamping the specimen–transducer sandwich (bonded with either silicon oil or carbon-impregnated model-making glue) in an encasing earthed metal holder. The resulting assembly has a complicated frequency resonance spectrum (irreproducible with specimen exchange), and one of the main resonances is usually chosen when imaging. For the 10 mm diameter transducers mostly used in our experiments these occur at about 200 kHz, whereas smaller diameter transducers in practice give higher frequency, sharper main resonances. For better resolution (§3) it is desirable to work at higher frequencies, but the higher Q-factors from small transducers may produce troublesome frequency sensitivities in the (phase-sensitive) images. The positioning of the transducer is not critical since the entire specimen is acoustically excited, and images have also been obtained with annular transducers mounted on either specimen surface.

The transducer signal is fed through a wideband, low-noise preamplifier chip to the main, lock-in amplifier with a reference wave derived from the chopping system. Such an amplifier simultaneously takes advantage of incoherent noise rejection, phase sensitivity, and the ability to 'tune' to harmonics of the reference frequency (used in the nonlinear images of §4*f*). An integration time constant of about 100 μs allows acceptable frame rates, with pixel dwell times usually of about the inverse of the acoustic resonance frequency bandwidth, so that mechanical ringing does not blur the image over several pixels.

A significant experimental drawback is that, to achieve measurable signal levels, electron-beam currents of the order of microamps are typical. This is difficult to achieve without some beam-spot size degradation, and it can also be a serious problem (though not an insuperable one (§4*d*)) with beam sensitive materials. The consequent temperature cycling amplitude under the beam may range from a few kelvins to about 100 kelvins, depending on the thermal properties of the specimen. This heating effect, together with a heating stage, has been used in preliminary observations of cyclic subsurface melting and solidification in Sn samples (D. R. Wright, unpublished results).

The main expense of the system is that of a commercial lock-in amplifier (especially for high-frequency, fast operation), although commercial complete SEAM systems make use of more economic, custom-made amplifiers.

3. Resolution and contrast

In general, resolution and contrast are derived from the small volume, close to the beam-entry surface, where the acoustic waves are generated. The incident electron beam, focused to a diameter D_0 less than 1 μm, deposits its energy in a roughly spherical volume of diameter D_s within the specimen. Solutions of the thermal diffusion equation for such a periodic heat source represent highly damped harmonic thermal waves which propagate for roughly one diffusion length, d_t, given by

$$d_t = (2K/\omega\rho C)^{\frac{1}{2}}, \tag{1}$$

where K is thermal conductivity, ω is 2π times chopping frequency, ρ is density, and C is specific heat capacity. Each point thus heated undergoes thermoelastic expansion and contributes to the final acoustic signal for any given beam position.

Lateral and depth resolution go hand in hand, and clearly the resolution depends on a combination of D_0, D_s and D_t $(= 2d_t)$, although it is mainly thermally limited for many materials. Representative values of D_s and $D_t = 2d_t$ are given in table 1 for a typical chopping

Table 1. Acoustic source parameters

material	Al	Cu	Au	Fe	Si	SiO_2	glass
D_s/μm	5	1.4	0.7	1.6	6	6	4 to 6
D_t/μm	22	24	25	10	8	1.8	≈ 2

frequency of 250 kHz and 30 keV beam energy. As confirmed experimentally (Balk *et al.* 1984*a*) there is considerable enhancement in resolution by increasing the chopping frequency into the megahertz range, at least for medium or good thermal conductors. In order to improve the resolution to 1 μm or less, D_s must also be decreased by lowering the accelerating voltage. The alternative procedure of using thin (less than 1 μm) specimens would introduce its own

problems of transducer mounting and fine-structure vibrational patterns (see §4*e*). Increased frequency and lower voltage both result in lower acoustic signal levels but despite this, sub-micrometre resolution will be an important experimental goal.

For the thermoelastic mechanism it is clear that the thermal expansion coefficient, α, will directly affect image contrast and for this reason, for instance, metal electrodes often image strongly against a semiconductor material. If the specimen is not thermally homogeneous, then changes in K may affect the temperature distribution of the source and also give rise to image contrast.

Different orientations of elastically anisotropic grains and also elastic discontinuities (such as cracks) close to the acoustic source both lead to interesting forms of contrast, which are discussed below. Changes in energy absorption due to surface topography provide only relatively weak contrast, so that in general little surface preparation is necessary.

As the next section will attempt to show, there is a growing body of evidence for non-thermoelastic generation mechanisms. These, and also nonlinear processes associated with signal generation, lead to enhanced resolution and offer alternative and unexpected sources of image contrast.

Contrast from one point on the specimen to another is generally due to both amplitude and phase differences (differential signal delays). The latter are observable with the phase-sensitive amplifier used, although absolute phase measurements are not significant as the vibrational modes induce full 2π phase variations, over a lateral scale of a few millimetres, which may be swept around the specimen in an unpredictable fashion by small changes of the chopping frequency. Because of this, images having phase contrast can show surprising changes in appearance with frequency variations of less than 1%.

4. Applications

(*a*) *Crystallographic contrast*

Images from polycrystalline specimens can show contrast from differently oriented grains (Cargill 1980*b*) as exemplified by figure 2, plate 1. The contrast between the large parent grains, as originally pointed out by Cargill (1980*b*), must be due to elastic anisotropy as other parameters, such as thermal conductivity, are scalars in cubic crystals. The highly elastically anisotropic, cubic Cu–Zn–Al alloy exhibits particularly good grain contrast whereas elastically isotropic tungsten has none. Contrast is much stronger than the weak channelling contrast often found in the secondary image, is independent of specimen tilt, and has been correlated with crystallographic orientation of the surface normal of the grains by Davies & Howie (1984) who presented a simple quantitative model which seems to agree with experiment. Qualitatively, the crystallographic dependence can be explained from the orientation affecting the acoustic output from the surface-constrained expansion of the small heated region, or at simplest the partition between in-plane and surface-normal expansions. This orientation-dependent strain produces a varying effect on the transducer signal via the selective excitation of various degenerate vibrational modes. This also means that highly frequency-dependent contrast in both amplitude and phase is found, since the vibrational characteristics are very sensitive to the chopping frequency.

An important point is that the characteristics of the available modes also depend strongly on the specimen mounting. This means that when a specimen is taken out and replaced, not only does the resonance spectrum from a given grain change, but also its signal amplitude and

PHILOSOPHICAL TRANSACTIONS OF THE ROYAL SOCIETY A MATHEMATICAL, PHYSICAL & ENGINEERING SCIENCES

particularly phase with respect to a neighbouring grain will be completely altered. Figure 3 shows spectra, taken with a stationary beam, from two neighbouring grains; the spectra taken after remounting cannot be identified with those taken before. Thus, although on average certain orientations produce stronger signals than others, absolute orientation determinations are, in practice, impossible by SEAM.

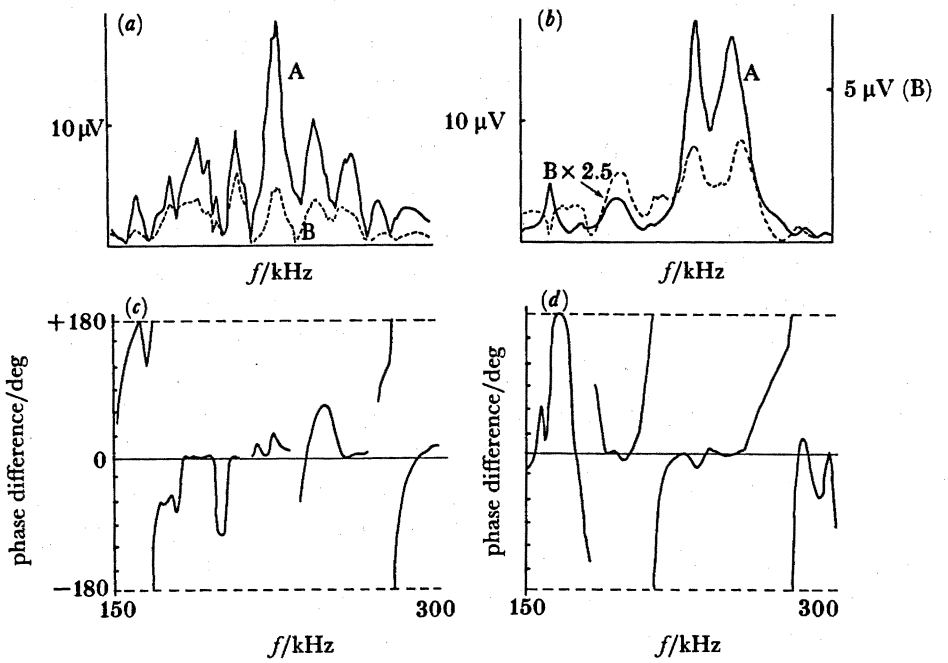

FIGURE 3. Results showing change of grain contrast after remounting specimen (of Cu–Zn–Al). (*a*) Amplitude spectra for two grains, A and B. (*b*) Amplitude spectra for same grains after remounting specimen. (*c*) and (*d*) Corresponding phase differences between A and B, before and after remounting. Curve is broken where signal was too low to define phase.

The specimen of figure 2 was plasma pitted in several places by a focused, high-power laser beam; topographic damage is visible in the secondary electron (SE) image, whereas it is obvious from the acoustic image that the affected area is much more extensive (white patches). The contrast in the laser pits is probably due to the formation of patches of a monoclinic martensite phase of the alloy under the heat and stress generated by the laser pulse. The martensite has quite different elastic and thermal properties from the parent phase, and has been shown to provide strong contrast in SEAM (Cargill 1980*b*; Davies 1983).

Looking again at figure 2 we can see some topographic contrast on the SE image at the etched grain boundaries. The acoustic image shows a localized contrast associated with the grain boundaries, and this also is very frequency dependent (Davies 1983). This is an example of the effect of a thermal and elastic boundary, which will be discussed more fully in §4*c* dealing with cracks.

(*b*) *Semiconductor materials*

SEAM is well suited to the study of semiconductor materials and devices, where information on layers and inhomogeneities down to depths of a few micrometres may be required, and where surface topography may be complicated.

In silicon, heavily doped regions and device layers have been imaged (Rosencwaig & White 1981; Davies 1983), with contrast attributable to thermoelastic variations. Because of the tend in VLSI technology towards submicrometre device thicknesses and ion implantations, it will become increasingly important to improve the lateral and depth resolution of the technique by using lower accelerating voltages and higher chopping frequencies.

In GaAs (Kirkendall & Remmel 1984) and in InP (Balk & Kultscher 1983) strong signals and rather interesting contrast are found. Figure 4, plate 1 shows part of a GaAs wafer (kindly supplied by M. Ridge of STC) where the SE image shows mainly surface metallizations. The GaAs not covered by the metallizations has been proton bombarded (at 50 keV, 2×10^{13} cm^{-2}) to form an amorphous layer about 1 μm thick. The acoustic image reveals a large irregular patch where the isolation was accidentally masked during processing as well as a rectangular masked patch (around one of the crosses) and small material inhomogeneities near and under the metallization. The property that produces the rather diffuse halo around the non-isolated region is not understood at present, but may be associated with process-induced strain. The resolution was measured to be 2–3 μm, *independent* of frequency down to about 15 kHz (below which the signal was too noisy for accurate data). This is a clear indication of a non-thermoelastic mechanism.

Images from semi-insulating GaAs wafers grown by the liquid encapsulated Czochralski (LEC) method show a network structure, as in figure 5, plate 1, which can be correlated with dislocations within the GaAs by X-ray topography (Rosencwaig 1984). We have found that this contrast is quenched if an Al electrode is evaporated onto the top (observed) surface of the specimen and then earthed. Contrast reappears if the electrode is floating, or if a negative voltage of more than about 5 V is applied to it. This seems to be further clear evidence that the images from GaAs are not due to the thermoelastic mechanism but are related to electrical effects, and this is supported by the similarity of the SEAM images of the networks to those generated from the charge collection from a surface electrode ('EBIC' type images). The dislocations have been found by other techniques (Nanishi *et al.* 1983) to be surrounded by electrically active impurity clouds. The piezoelectric nature of crystalline GaAs may be important in coupling electron–hole generation to acoustic waves, with the carrier generation being dependent on the electrical condition of the surface. In some cases decreasing the electron beam current results in an inversion of the contrast of the networks, and this may provide some clue as to their electrical effect.

Clearly, with the complexity of physical properties demonstrated by semiconductor specimens

---

DESCRIPTION OF PLATE 1

All images taken at 30 keV accelerating voltage, and f between 200 kHz and 300 kHz, unless otherwise stated.

FIGURE 2. (*a*) SE and (*b*) SEAM images of a laser-pitted polycrystalline Cu–Zn–Al specimen (see text).

FIGURE 4. (*a*) SE and (*b*) SEAM images of proton-implantation and other features on a GaAs wafer.

FIGURE 5. SEAM image of dislocation network in a GaAs wafer. The specimen was polished, and featureless in the SE image.

FIGURE 6. SEAM image of arcs of plastic deformation induced by machining a polycrystalline Cu specimen. The specimen had been electropolished, and was featureless in the SE image.

FIGURE 7. (*a*) SE and (*b*) SEAM image of an Al–Si–C specimen with voids, clearly linked by a crack in the SEAM micrograph.

PHILOSOPHICAL TRANSACTIONS OF THE ROYAL SOCIETY A MATHEMATICAL, PHYSICAL & ENGINEERING SCIENCES

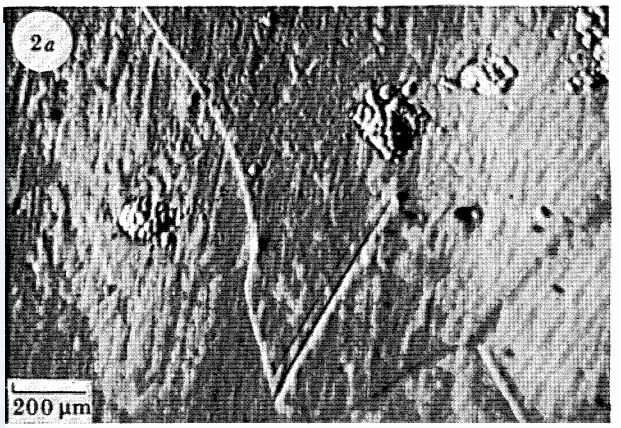

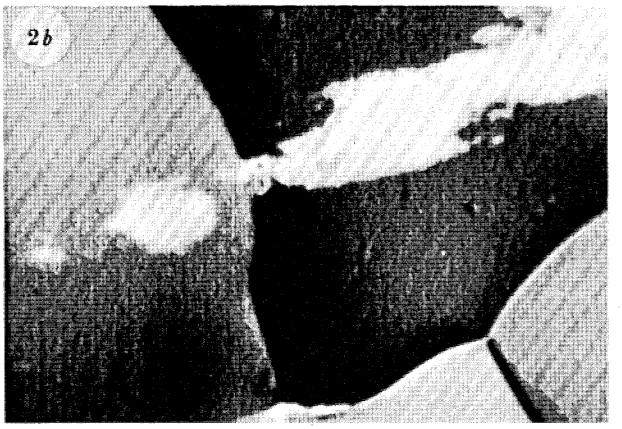

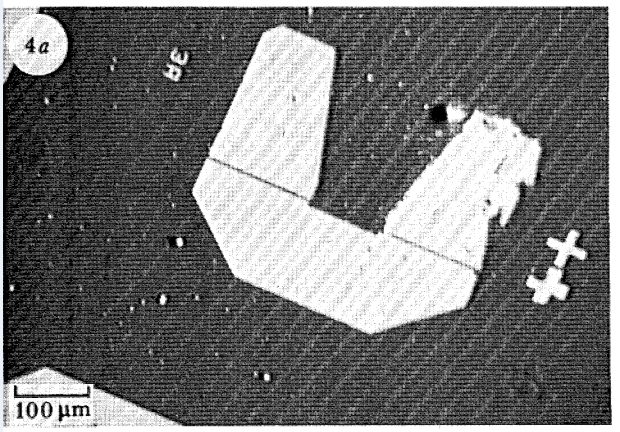

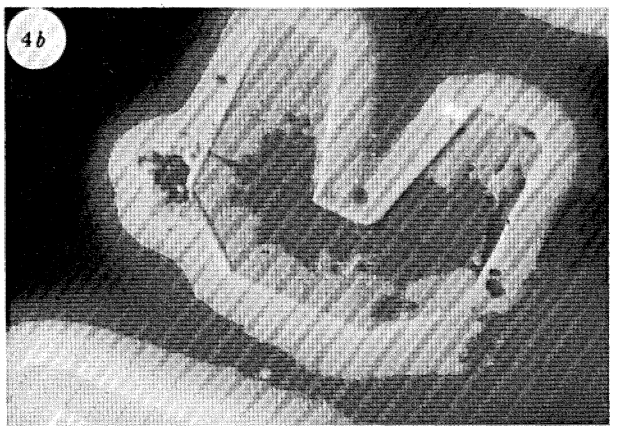

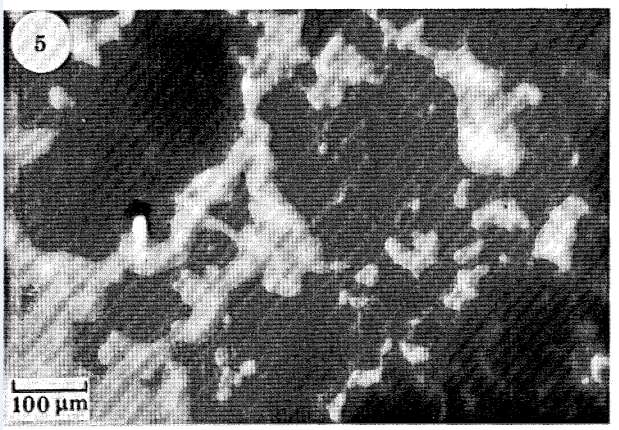

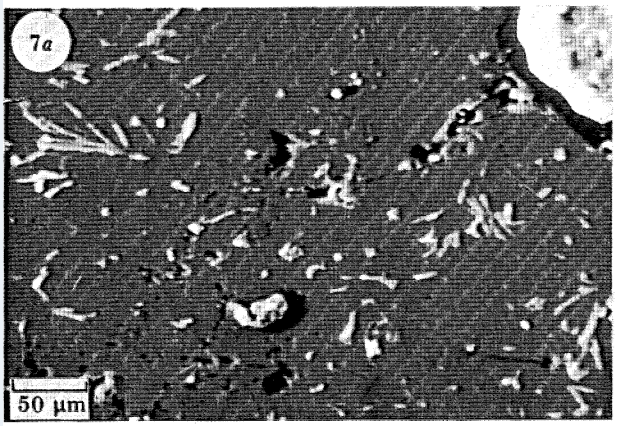

FIGURES 2 AND 4–7. For description see opposite.

(*Facing p.* 248)

PHILOSOPHICAL TRANSACTIONS OF THE ROYAL SOCIETY A MATHEMATICAL, PHYSICAL & ENGINEERING SCIENCES

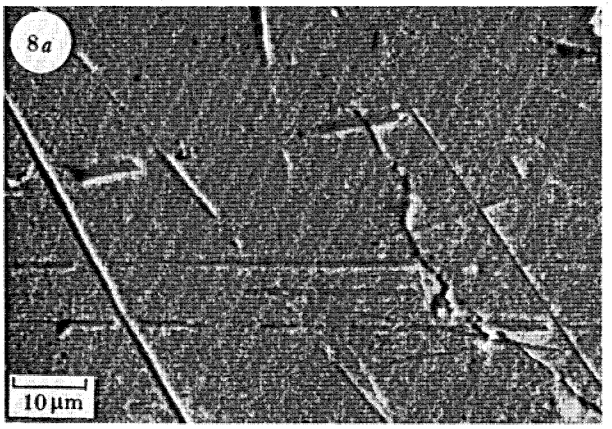

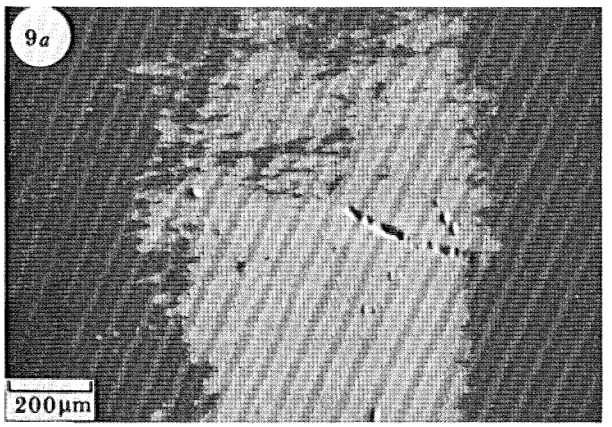

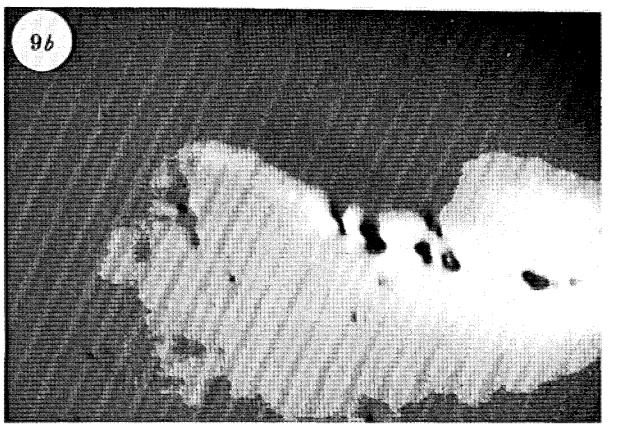

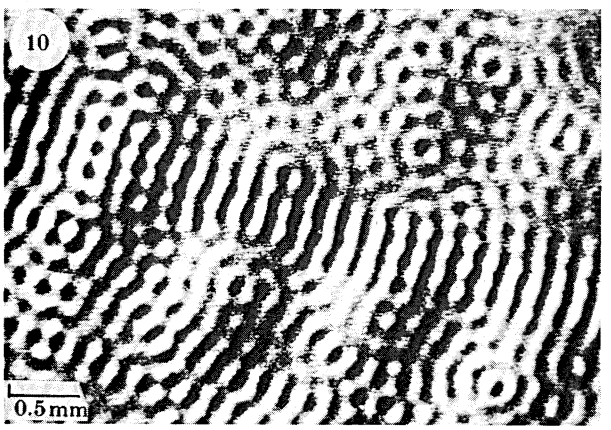

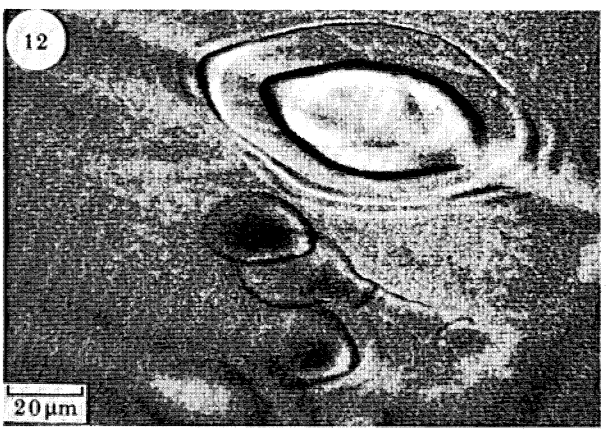

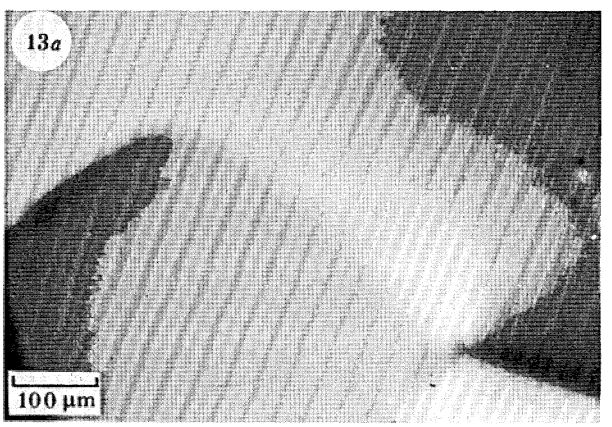

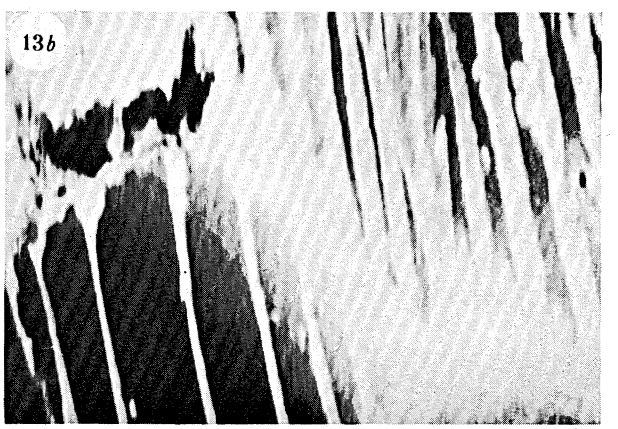

FIGURES 8–10, 12 AND 13. For description see opposite.

PHILOSOPHICAL TRANSACTIONS OF THE ROYAL SOCIETY A MATHEMATICAL, PHYSICAL & ENGINEERING SCIENCES

there is still considerable uncertainty of interpretation. Nevertheless, there are obvious practical applications for the ability to image such features as doped regions or electrically active impurity networks.

(*c*) *Deformation and cracks*

In GaAs we have seen individual grown-in dislocations. Cargill (1980*b*) showed that, in Cu, regions of high plastic deformation could provide image contrast such as that of figure 6, plate 1, which shows the result of machining damage to a Cu specimen. The arced regions here obviously represent dense masses of dislocation tangles, and individual dislocations are not imaged. Cargill originally proposed that the mechanism was a change in thermal conductivity due to increased phonon scattering at the dislocations. In metals at room temperature, however, this is likely to be a small effect. It seems more likely that a change in elastic properties, known as the modulus defect, may account for the contrast. This elastic change is due to the dynamic bowing of dislocations with the passage of any elastic wave, and it produces a change both in stiffness and in damping (Pollard 1977). An important objection is that the effect would be quenched by pinning due to point defects (at relatively low concentrations) for the passage of waves with low strain amplitude (below about 10^{-6}). However, for amplitudes sufficiently high to drive the dislocations over the pinning points, the modulus defect may be as large as several percent. Directly under the beam the elastic strain amplitude may be as high as 10^{-4}, so this mechanism may well be dominant. The modulus defect at high amplitude is dependent on the pinning point density, and this may explain why we have not been able to image regions of more controlled localized damage in much purer Cu specimens. It also indicates that the technique may be of erratic applicability in examining plastic deformation in other types of specimens.

Figure 7, plate 1, demonstrates the effectiveness of SEAM for detecting discontinuities in the specimen surface, in this case small voids which can be seen to be joined together by a long crack in an Al–Si–C alloy. Figure 8, plate 2, shows an example of the detection of an apparently non-surface-breaking crack in an Fe–Ni–C alloy, and images of cracks in non-metals appear elsewhere (Davies 1983; Rosencwaig 1984). In general the contrast around the crack occurs on a scale of about 15–100 μm at frequencies of about 250 kHz, with little systematic variation between different types of conductor. The contrast mechanism must involve the crack acting to scatter both thermal *and* acoustic waves; if only thermal wave reflection were important then no contrast would be seen at a crack, as the thermoelastic stress would be simply integrated over the heated volume to give the acoustic signal, and the results would be identical for a

---

DESCRIPTION OF PLATE 2

FIGURE 8. (*a*) SE image of a crack in an Fe–Ni–C alloy. (*b*) SEAM image reveals subsurface crack extending beyond visible crack tip, and also a second, completely subsurface crack.

FIGURE 9. (*a*) SE image of a crack in polystyrene and (*b*) SEAM image showing craze extending beyond the crack tip. The specimen was Cu-coated and imaged at 20 keV to avoid degradation.

FIGURE 10. SEAM image showing vibrational pattern in a smooth, 16 μm thick Al foil at $f = 5.8$ MHz. The pattern has short wavelength (A) and long-wavelength (S) Lamb modes superimposed.

FIGURE 12. $2f = 220$ kHz nonlinear SEAM micrograph showing very fine ring features associated with martensite platelets in a Cu–Zn–Al alloy.

FIGURE 13. (*a*) Normal SEAM image showing only grain structure of a polished Fe–Si transformer sheet. (*b*) $2f = 253$ kHz nonlinear image of the same region reveals magnetic domain structures.

PHILOSOPHICAL TRANSACTIONS OF THE ROYAL SOCIETY A MATHEMATICAL, PHYSICAL & ENGINEERING SCIENCES

normally propagating thermal wave or for one reflected back upon itself (Davies *et al.* 1983). Thus we must conclude that points near a free surface must have different acoustic importance from those far away, leading to a different integrated final outgoing stress wave in the two cases.

Similar principles, of course, apply to the imaging of a less dramatic interface such as a grain boundary. Actually, this condition of different acoustic weighting for different distances from an interface, in particular depth from the specimen surface, can be shown to be a necessary one for the imaging of any type of thermal variation (Davies 1983). For crack imaging in SEAM it would appear that the width between the crack walls need only be the nanometre or so needed to destroy mechanical and thermal conductivity. However, it seems that the total side-on area (length by depth) should be at least comparable to the cross section of the heated region in order for the crack to influence a significant proportion of the outgoing wavefront. This conclusion is supported to some extent by the poor SEAM imaging of cracks in a 10 μm TiN coating (hence only 10 μm deep) which were well imaged by conventional scanning acoustic microscopy (Briggs 1984).

(*d*) *Beam sensitive materials*

For materials such as polymers or biological specimens it is obvious that a several-microamp electron beam at 30 keV will be anything but non-destructive. However, such specimens can be examined in SEAM by the use of an electron-opaque coating which nevertheless allows significant heating effect to be passed into the main sample. For up to 30 keV a suitable coating is about 1.5–2 μm of Cu, and this has enabled the imaging of a crack and its precursor (a craze) in polystyrene (figure 9, plate 2). There is no noticable degradation even on sustained examination, and other specimens successfully imaged include fibre-reinforced poly-ether-ether-ketone (PEEK) polymer and resin-coated photographic paper. Although biological specimens will provide their own problems of transducer mounting and vacuum sensitivity, it seems only a matter of time before SEAM is being used to examine their thermal and elastic microstructure.

(*e*) *Vibrational patterns*

Vibrational patterns show that acoustic-propagation properties can produce strong amplitude and phase contrast, and they are always present because of the repetitive excitation used in SEAM. Their size depends mainly on the specimen thickness and the chopping frequency, and under normal conditions their potentially confusing effect on the image can be minimized by slight frequency tuning until the area of interest lies entirely within one antinode of the pattern, as is the case with most of the images presented here. Although the patterns may initially appear to be of rather limited interest, their study reveals useful information on the type of acoustic waves generated in the specimen, and they are also the basis of a useful application because they offer the possibility of information from depths of millimetres rather than micrometres, albeit with consequently poorer resolution.

Detailed study has shown that the patterns correspond to plate excitations known as Lamb waves, which have complicated dispersion curves (Auld 1973) falling into two classes: excitations that are either antisymmetric (A) or symmetric (S) about the specimen mid-plane. The two lowest theoretical Lamb dispersion curves (in ω, k space) are most physically significant; at low frequencies (compared with the fundamental specimen thickness shear resonance) the A and S excitations resemble classical flexural and dilatational waves respectively, while at high frequencies the two dispersion curves converge on Rayleigh surface-wave

PHILOSOPHICAL TRANSACTIONS OF THE ROYAL SOCIETY A MATHEMATICAL, PHYSICAL & ENGINEERING SCIENCES

behaviour. We have experimentally confirmed (Davies 1985) the presence of these lowest A and S excitations in both low and high frequency régimes, although the A branch appears to be dominant in thick (of the order of millimetres) specimens at low frequencies (less than 2 MHz). Figure 10, plate 2 shows a clear example of the A and S modes at a frequency where they have quite different wavelengths (which are rather small in the thin foil).

The thickness sensitivity can be used to detect deep delaminations because the delaminated portion of the specimen will vibrate with a shorter wavelength pattern, as shown in the schematic of figure 11, and demonstrated by Rosencwaig (1983) for die-bonding of an IC chip. Unfortunately, because the dispersion curves tend to straight lines (thickness-independent Rayleigh waves) at high frequencies, this application will only be feasible where the depth of the delamination does not exceed, roughly, its width (parallel to the surface). Of course the resolution is limited to roughly one wavelength of the pattern over the delamination. Vibrational patterns on contact wires to ICs (Davies 1983) might also be used as indicators of wire-bonding integrity.

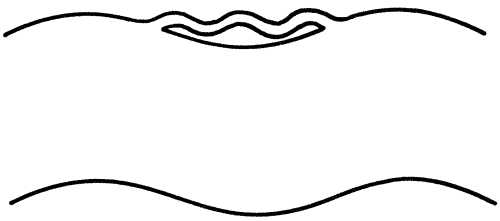

FIGURE 11. Schematic of the detection of a delamination in the specimen by a change in vibration-pattern wavelength.

The vibrational patterns explain why smaller transducers produce stronger signals at high frequencies than do large ones; it is because a large transducer will experience cancelling signals if it covers many positive and negative antinodes of the specimen pattern. Thus either the transducer should be matched roughly to the mode wavelength in the desired frequency range, or elaborate phase-shifted transducer arrays may have to be used.

(*f*) *Nonlinear imaging*

Nonlinear processes in any of the signal generation mechanisms should lead to signals at harmonics of the chopping frequency, and these may be used to form so called nonlinear images (Balk & Kultscher 1983) by tuning the lock-in amplifier to even harmonics of the chopping frequency, f. Odd harmonics are not used as they are contained as Fourier components of the primary excitation waveform for a square-wave chop, and in practice $2f$ is the easiest signal to obtain.

For most specimens there are no measurable $2f$ signals but in some special cases $2f$ images can be formed, and they show substantial improvements in resolution over the normal, f, images as well as new forms of contrast (Balk *et al.* 1984*b*). This can be seen in figure 12, plate 2, which is an example of the very fine ring structures (much more closely-spaced than a thermal wavelength) formed in $2f$ images of martensite platelets in a Cu–Zn–Al alloy. By scanning the chopping frequency down with the detection frequency fixed (for several experimental reasons this is very much simpler than scanning the detection frequency up) we have been able to obtain quantitative data on the harmonic content of the signal coming from a point within

the ring system. This is displayed in table 2 in terms of percentages of the fundamental component, and there is clear evidence for strong harmonic generation.

The current proposal for the harmonic generation in the Cu–Zn–Al is that the martensite, which is unstable to temperature and stress, is cyclically (but hysteretically) growing and shrinking at the tip under the periodic influence of the beam. The growth is likely to be nonlinear because of the presence of microstructural defects or crystallographic variants, along the length of the platelet, which would impede the cycling. Each ring in the image would thus correspond to the locus of electron beam positions from which each such defect is encountered by the thermal cycling.

TABLE 2. HARMONIC CONTENT OF SIGNAL FROM MARTENSITE TIP

harmonic	f	$2f$	$3f$	$4f$	$5f$	$6f$	$7f$	$8f$
martensite tip	100	50	42	24	22	19	18	15
chopping waveform	100	0.7	29	0.6	13	0.4	7	0.3

accuracy *ca.* ± 10% of absolute value.

The rings in the Cu–Zn–Al specimen are perhaps just a curiosity, but figure 13, plate 2 (taken at the University of Duisburg with L. J. Balk and N. Kultscher) shows how magnetic domains may be imaged by the $2f$ mode in transformer sheet material, while the normal f image reveals only the grain structure. The resolution at $2f$ is here found to be of the order of 1 μm, again much smaller than a thermal wavelength. Several observations support the supposition that magnetic domains are being imaged here, including growth and rotation of the features in an externally applied, rotated magnetic field (L. J. Balk, personal communication). The contrast mechanism is not yet clear but, by analogy with the proposal for Cu–Zn–Al, it probably involves acoustic emission from Barkhausen-type movement of the domain walls under the stress or perhaps the magnetic field caused by the electron beam (although we would expect the latter to be very weak).

Nonlinear signals might also be useful in the type of experiment, mentioned earlier, which attempts to detect subsurface nucleation of melting in solid Sn samples.

5. OTHER FORMS OF MICROSCOPY

A new technique such as this will only be really useful if it provides information more easily than, or exclusive to, other methods. The more established field of scanning acoustic microscopy (SAM) gives elastic information at high resolution which in many cases results in similar images to SEAM. However, from this and other papers presented at this meeting it should be clear that contrast mechanisms are never entirely the same in the two techniques so that, as pointed out by Briggs (1984), they are essentially complementary. The advantages of SEAM are that it is relatively cheap to install on the large number of existing SEMs, it has immediately available for comparison all the other imaging and analytical modes of the SEM, and it is much less sensitive to rough-surface topography than SAM. The disadvantages are that it must be performed *in vacuo* with an electron beam which can cause considerable damage to some specimens. In both techniques image interpretation is complicated; SEAM has ambiguity between thermal and elastic effects, SAM between elastic changes and surface topography, although imaging theory is more advanced for SAM.

Some of the experimental disadvantages of SEAM could be eliminated by moving to chopped optical (laser) induced acoustic microscopy. Indeed, because of the very short absorption distance for light in many specimens and the high chopping frequencies attainable, D_s and D_t can be made very short, and sub-micrometre (particularly depth) resolution may be more easily attained. If in such a system the so-called 'thermoacoustic' signal generated in a gas cell surrounding the specimen is detected, then purely thermal images may be obtained, as this signal is a measure of the average temperature of the specimen surface. Images formed from such a signal would no doubt resolve some of the thermal–elastic ambiguity of the thermoelastic technique.

6. Conclusions

SEAM has been able to provide interesting data which is of use in a variety of materials science applications such as the imaging of polycrystalline structure, dopants and inhomogeneities in semiconductor materials, cracks, delaminations, and magnetic domain patterns. Resolution is currently of the order of several micrometres but sub-micrometre resolution seems attainable, and information is obtained down to a comparable depth, which may be varied by large frequency changes. Much of the physics of the contrast mechanisms is now clear, though there is as yet no detailed quantitative understanding because of such factors as the difficulty in quantifying the effect of elastic boundary conditions on the final vibrations established in the specimen. The importance of non-thermoelastic mechanisms has been established in many cases. Future progress will involve the use of higher frequencies and more elaborate transducer systems, examination of biological specimens, and comparative work with scanning laser systems.

The strength of the SEAM technique lies not in some unique application, but rather in its usefulness in a wide range of problems. The technique has now reached a level where it cannot safely be ignored by the SEM user.

I thank Dr A. Howie, F.R.S., for his unerring insight and his careful guidance. I also thank Dr L. J. Balk and Dr G. A. D. Briggs for discussions and for their support. The SERC and the Master and Fellows of St Catharine's College, Cambridge have provided me with a Research Fellowship and numerous material benefits, and I gratefully acknowledge their generosity.

References

Auld, B. A. 1973 *Acoustic Fields and Waves in Solids*, vol. II. New York: John Wiley and Sons.
Balk, L. J. & Kultscher, N. 1983 Microscopy of semiconducting materials. In *Institute of Physics Conference Series*, no. 67, pp. 387–401. London: Institute of Physics.
Balk, L. J., Davies, D. G. & Kultscher, N. 1984*a* *Physica Status Solidi* A **82**, 23–33.
Balk, L. J., Davies, D. G. & Kultscher, N. 1984*b* *Scanning Electron Microscopy*. **III**, 1601–1610.
Brandis, E. & Rosencwaig, A. 1980 *Appl. phys. Lett.* **37**, 98–100.
Briggs, G. A. D. 1984 *Scanning Electron Microscopy* **III**, 1041–1052.
Cargill, G. S. 1980*a* *Nature, Lond.* **286**, 690–693.
Cargill, G. S. 1980*b* In *Scanned image microscopy* (ed. E. A. Ash), pp. 319–330. London: Academic Press.
Davies, D. G. 1983 *Scanning Electron Microscopy* **III**, 1163–1176.
Davies, D. G. 1985 Scanning electron acoustic microscopy. Ph.D. thesis, University of Cambridge.
Davies, D. G. & Howie, A. 1984 Electron microscopy and analysis. In *Institute of Physics Conference Series*, no. 68, pp. 467–470. London: Institute of Physics.
Davies, D. G., Howie, A. & Staveley-Smith, L. 1983 *J. Soc. Photo-Opt. Instrum. Engrs* **368**, 58–68.
Kirkendall, T. D. & Remmel, T. P. 1984 *J. Phys., Paris* C **45**, 877–880.

PHILOSOPHICAL TRANSACTIONS OF THE ROYAL SOCIETY A MATHEMATICAL, PHYSICAL & ENGINEERING SCIENCES

Menzel, E. & Kubalek, E. 1979 *Scanning Electron Microscopy* **I**, 305–317.
Nanishi, Y., Ishida, S. & Miyazawa, S. 1983 *Jap. J. appl. Phys.* **22(1)**, 54–56.
Pollard, H. F. 1977 *Sound waves in solids*. London: Pion Ltd.
Rosencwaig, A. 1980 In *Scanned image microscopy* (ed. E. A. Ash), pp. 291–317. London: Academic Press.
Rosencwaig, A. 1983 *J. Phys., Paris* C **44**, 437–452.
Rosencwaig, A. 1984 *Scanning Electron Microscopy* **IV**, 1611–1628.
Rosencwaig, A. & White, R. M. 1981 *Appl. phys. Letts.* **38**, 165–167.

Discussion

R. E. Green (*Center for Nondestructive Evaluation, The Johns Hopkins University, Baltimore, Maryland, U.S.A.*). Dr Davies stated that when he took his specimens out of the scanning electron microscope and then replaced them, that he obtained completely different irreproducible results. Did he remove the Cu–Zn–Al polycrystal from the piezoelectric crystal to which it was acoustically coupled when he took it out of the electron microscope? If so, this explains why he did not obtain reproducible results. If he had left the specimen permanently attached to the piezoelectric crystal then his results would have been the same when he replaced the specimen–crystal combination back in the electron microscope. The reason removing the Cu–Zn–Al specimen from the piezoelectric crystal gives irreproducible results is that it is virtually impossible to acoustically couple the specimen to the piezoelectric crystal in a repeatable fashion and, therefore, the acoustic impedance associated with this coupling changes so drastically that irreproducible results are obtained. My colleagues at Johns Hopkins have conducted similar experiments and they are able to obtain reproducible results every time, provided that they take the precautions stated above.

D. G. Davies. Yes, the transducer was simply bonded with oil, and was detached and then replaced. Bonding irreproducibility undoubtedly has a large effect, and the importance of the result is that far-field acoustic conditions can superimpose highly frequency-sensitive contrast effects on those attributable to material parameters within the generation volume. The real concern is not reproducibility, but *predictability*, and the experiment was performed to demonstrate that any exact theoretical description of signal contrast must include a model of the specimen mounting, a difficult task.

M. Somekh (*Department of Metallurgy and Science of Materials, University of Oxford, U.K.*). Is there any effect if one uses a shear-wave transducer?

D. G. Davies. The PZT transducers used are sensitive to both longitudinal and shear waves. However, because we use cyclic rather than single-pulse sources (and detectors), the acoustic excitations must be described in terms of the steady-state superposition of all the (mode-converted) reflections within the specimen, i.e. in terms of the Lamb waves. It would only be meaningful to distinguish shear from longitudinal waves by using single-shot, time-resolved measurements.

R. E. Green. I disagree with the statement that there is no unique depth resolution with the scanning electron acoustic microscopy technique, because by proper choice of electron beam voltage and chopping frequency it is possible to image various planes in a multi-layer silicon crystal layer by layer in a controlled fashion. This makes the scanning electron acoustic microscope an extremely valuable tool for nondestructive evaluation of a variety of very large-scale integrated (VLSI) circuit devices.

PHILOSOPHICAL TRANSACTIONS OF THE ROYAL SOCIETY A MATHEMATICAL, PHYSICAL & ENGINEERING SCIENCES

D. G. Davies. Successively thicker layers can be sampled by expanding the thermoelastic generation volume (e.g. by lowering the chopping frequency) and, in this sense, some depth probing is certainly possible, although a true 'profile' would have to be mathematically extracted from the data. However, for any one fixed frequency it is misleading to attach specific depth to features imaged at some particular phase, because feature depth and signal phase are not likely to be either unambiguously or montonically related for a non-homogeneous sample.

G. Busse (*I.K.P., Universität Stüttgart, F.R.G.*). Compared with a laser beam, an electron beam not only produces heat, but also injects charges. This effect does not seem to be obvious. From the low energy input and the good signal: noise ratio, I assume that the signal per energy input is much higher than for optically generated waves. This indicates that other signal generating mechanisms are involved in such way that only a small part of your signal is related to thermal waves. By using other kinds of detection it should be possible to analyse the various contributions.

D. G. Davies. Indeed, and Dr Busse is right to infer that in many of the cases presented here (e.g. GaAs) a simple thermal-wave treatment will not suffice. Comparison with images from the purely thermal-wave techniques, such as those which he operates, will be extremely useful in identifying non-thermoelastic mechanisms.

PHILOSOPHICAL TRANSACTIONS OF THE ROYAL SOCIETY A MATHEMATICAL, PHYSICAL & ENGINEERING SCIENCES

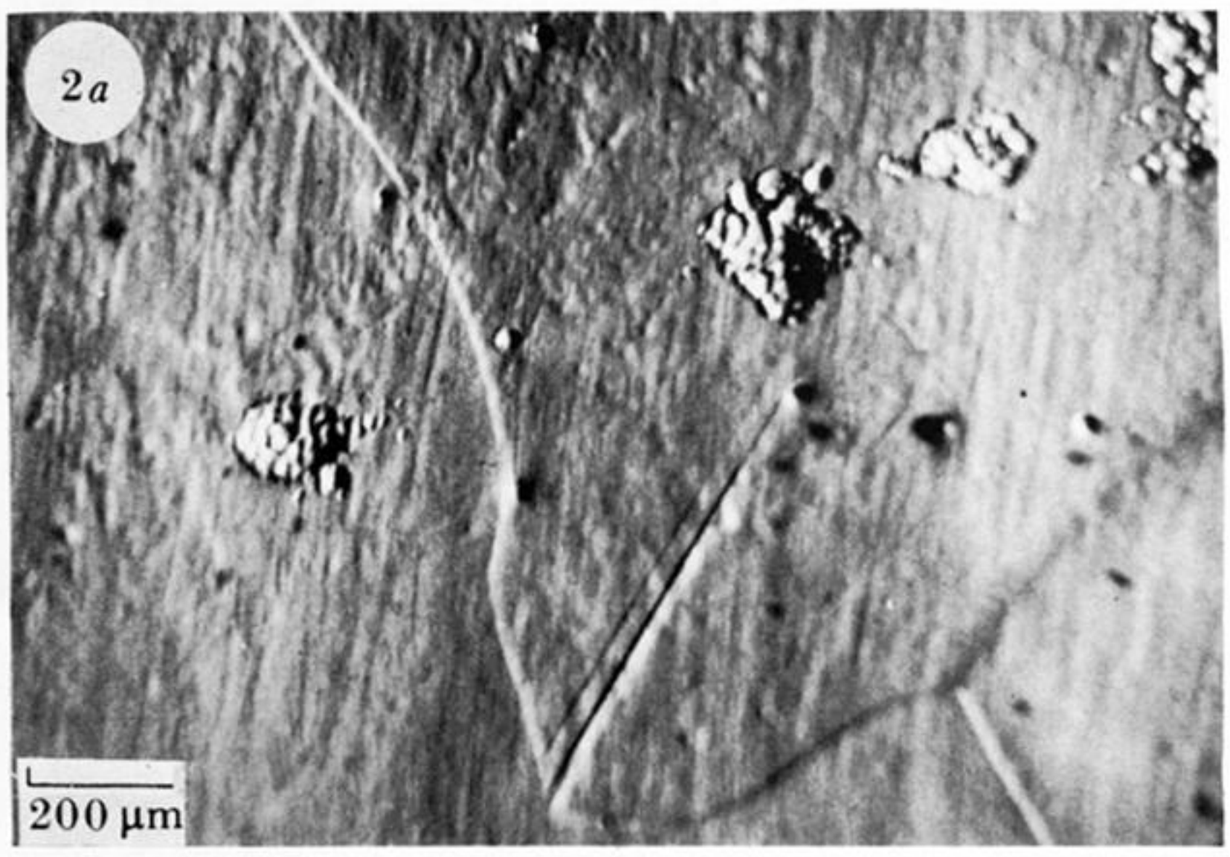

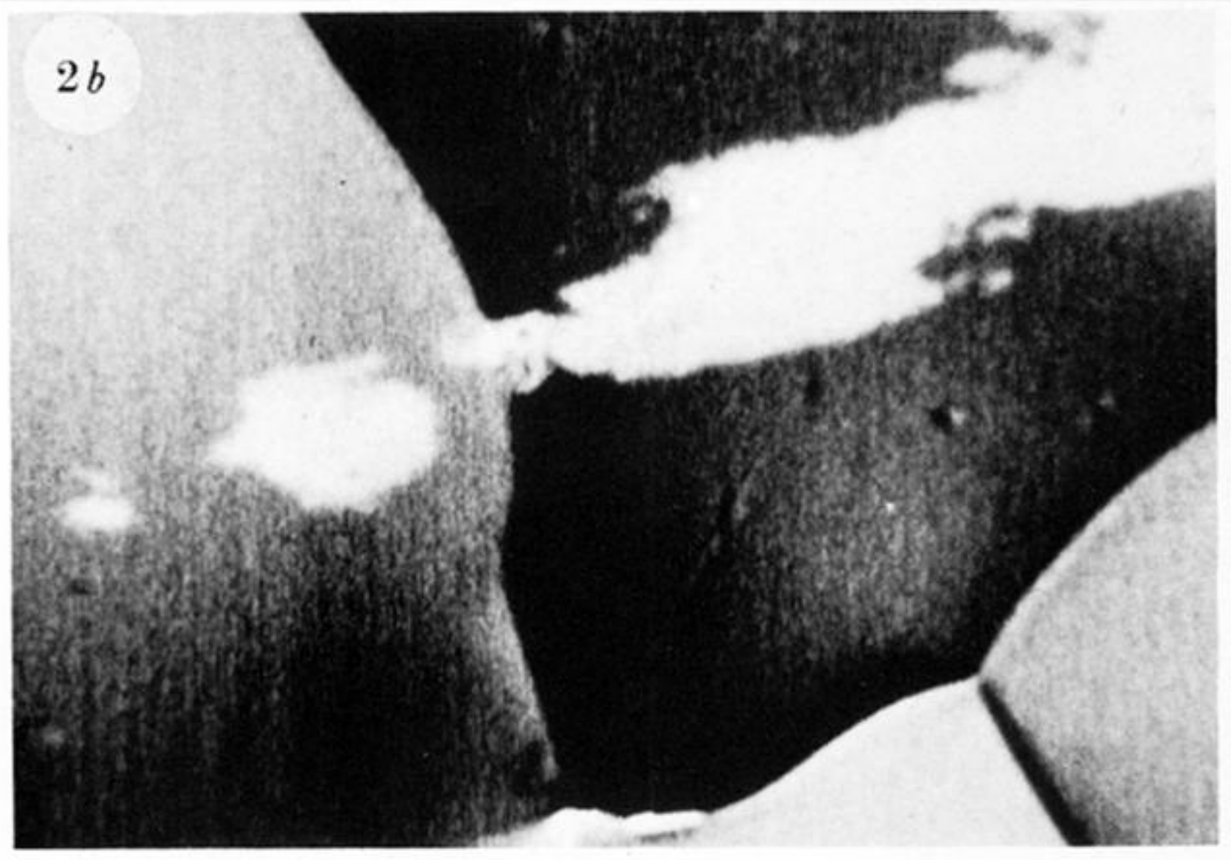

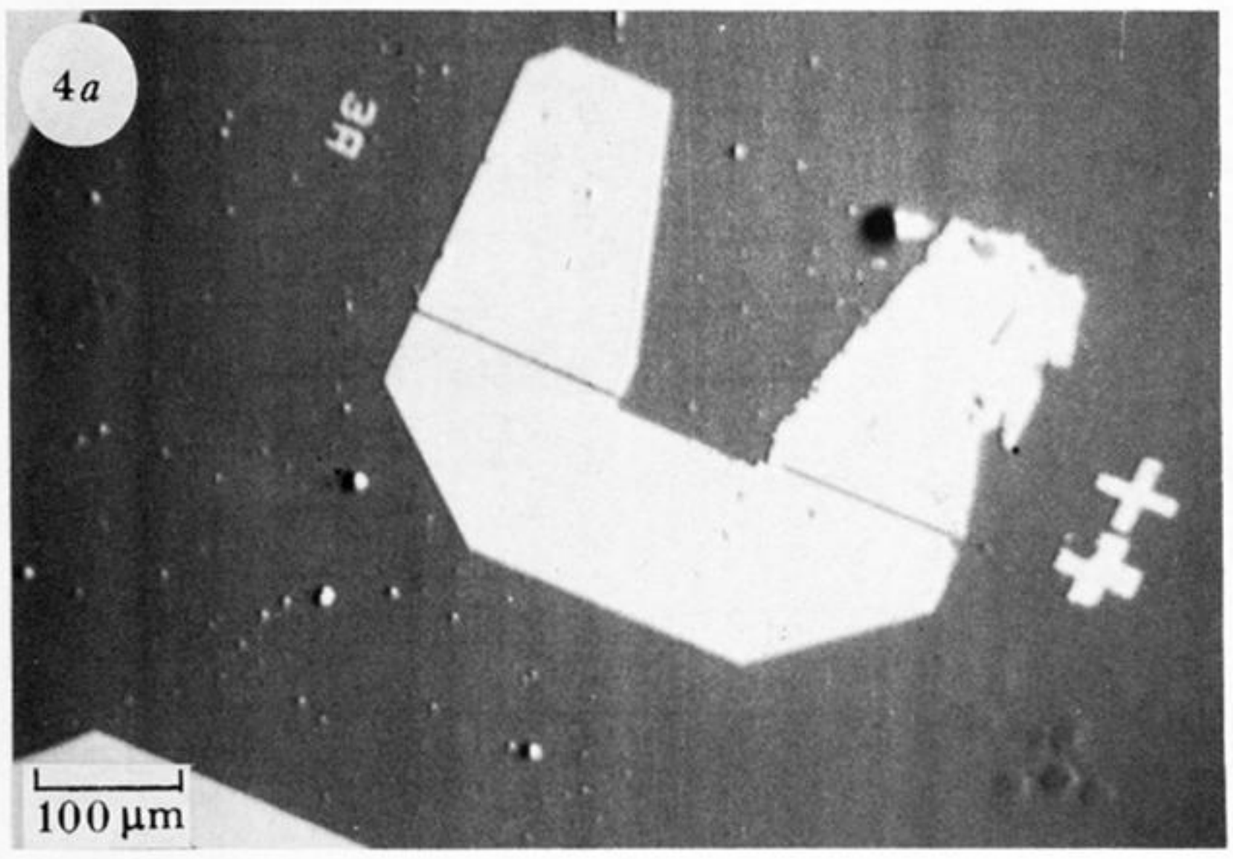

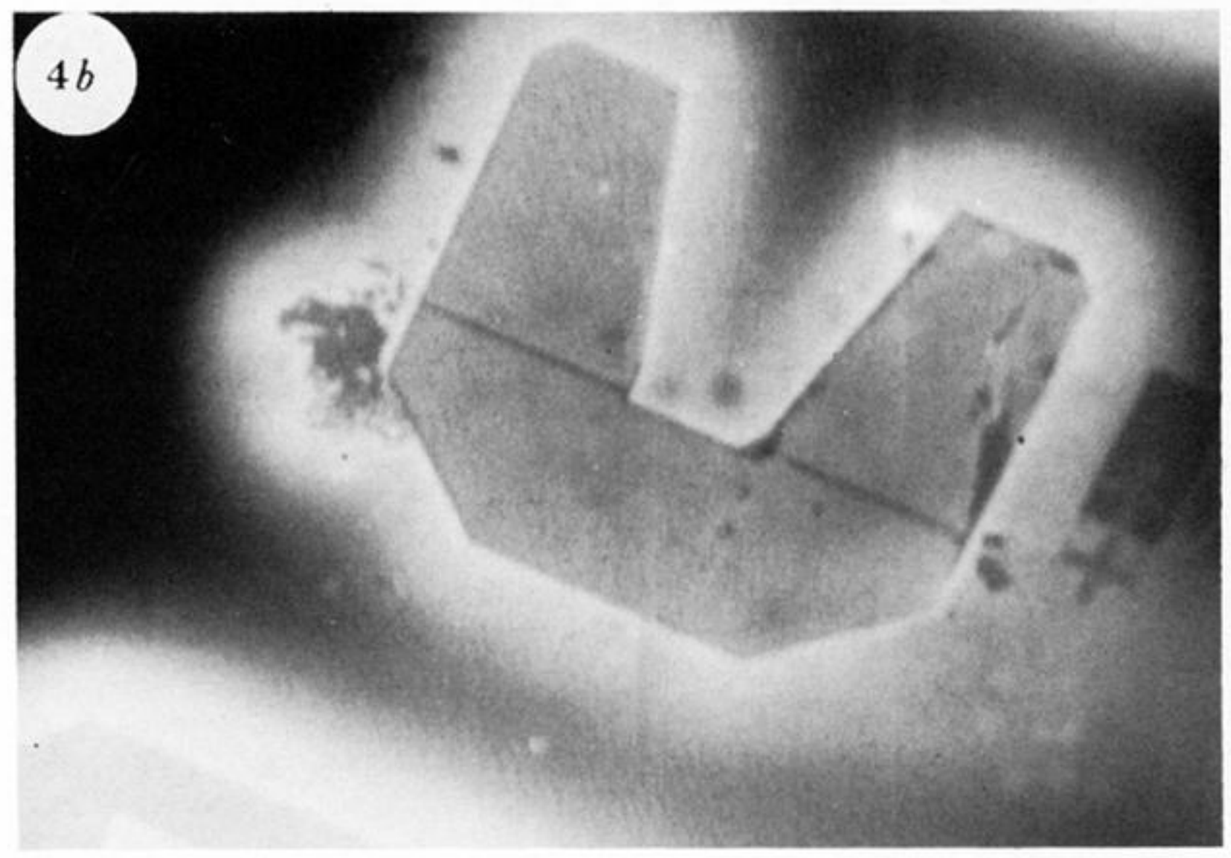

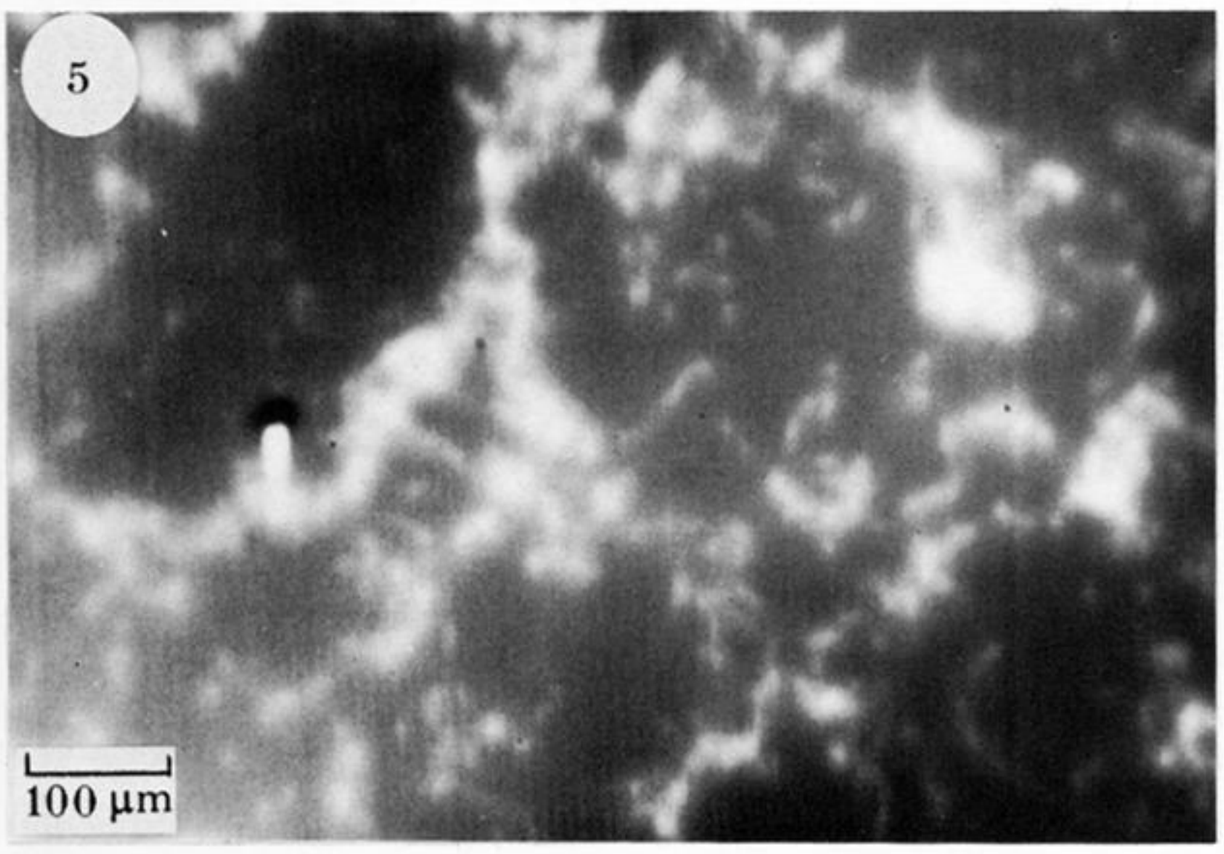

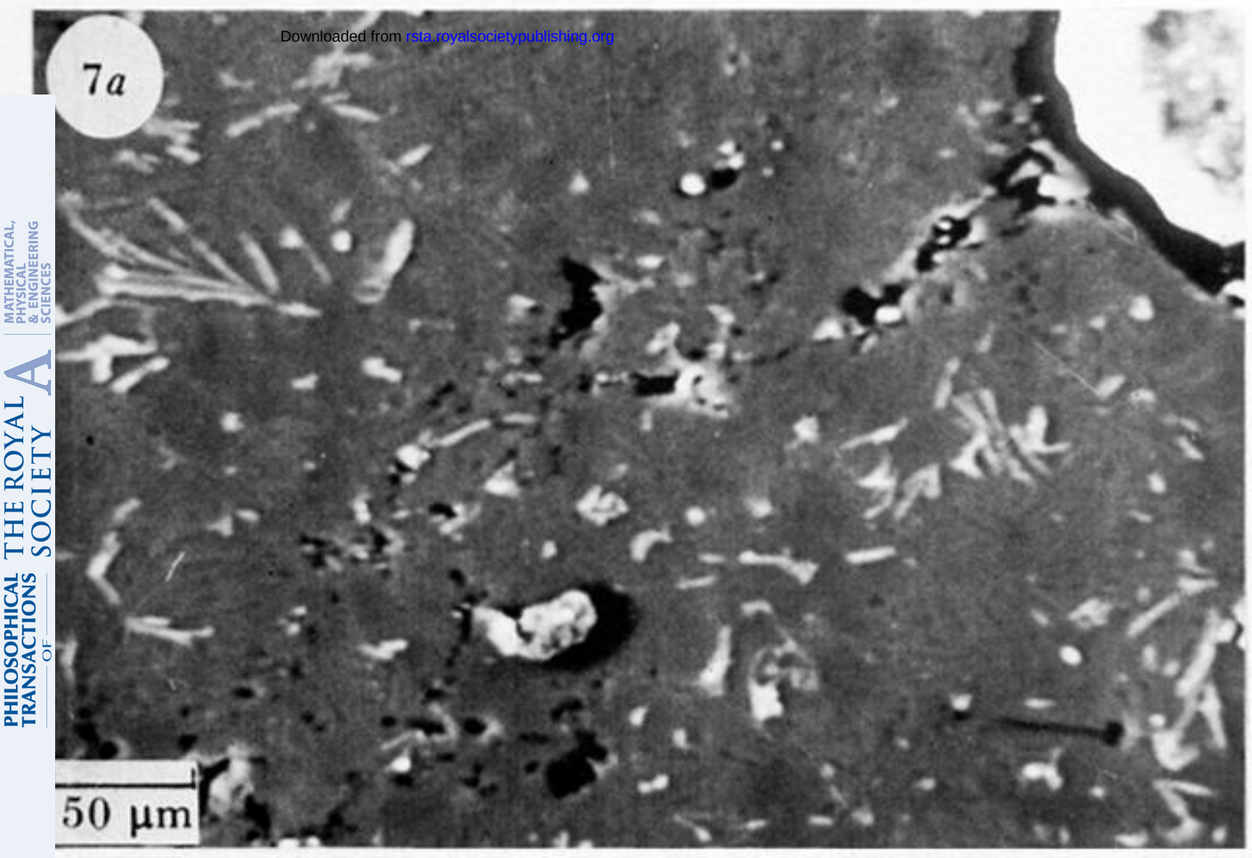

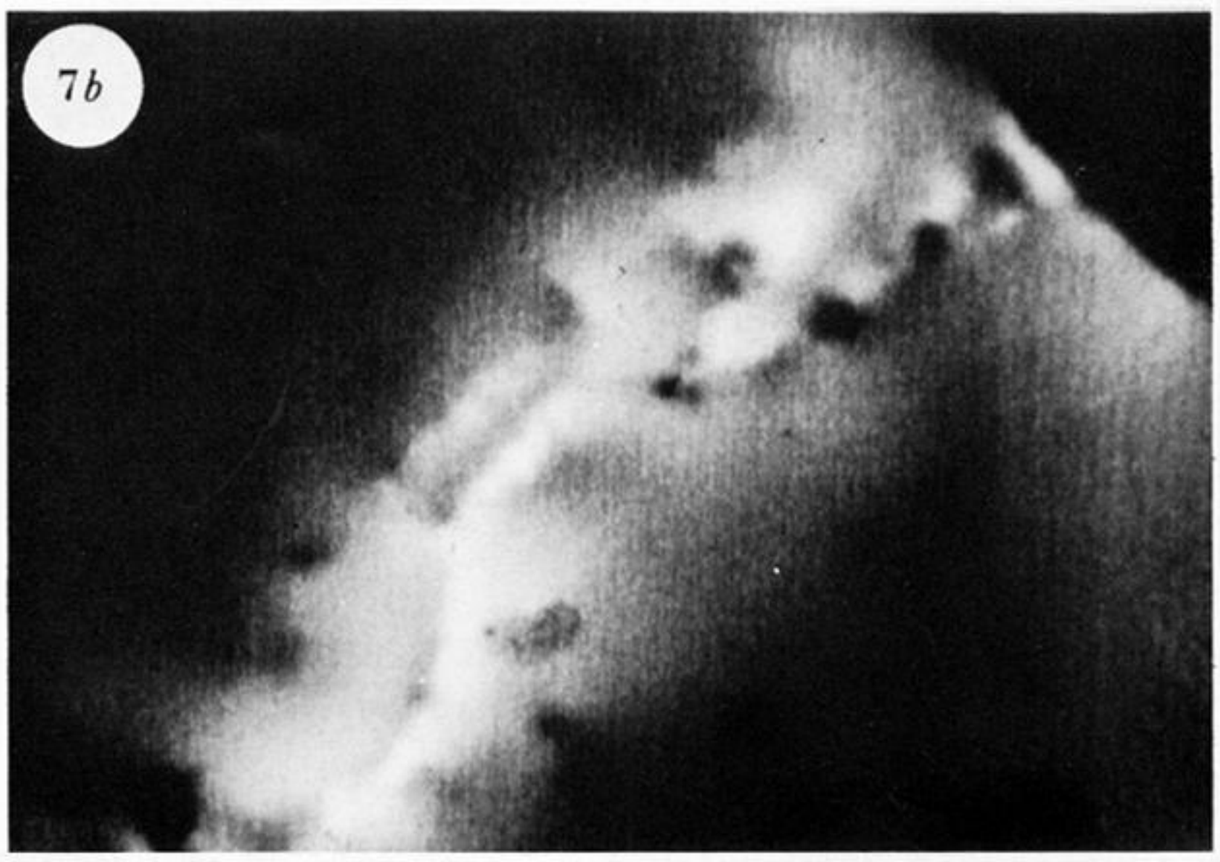

All images taken at 30 keV accelerating voltage, and f between 200 kHz and 300 kHz, unless otherwise stated.

FIGURE 2. (*a*) SE and (*b*) SEAM images of a laser-pitted polycrystalline Cu–Zn–Al specimen (see text).

FIGURE 4. (*a*) SE and (*b*) SEAM images of proton-implantation and other features on a GaAs wafer.

FIGURE 5. SEAM image of dislocation network in a GaAs wafer. The specimen was polished, and featureless in the SE image.

FIGURE 6. SEAM image of arcs of plastic deformation induced by machining a polycrystalline Cu specimen. The specimen had been electropolished, and was featureless in the SE image.

FIGURE 7. (*a*) SE and (*b*) SEAM image of an Al–Si–C specimen with voids, clearly linked by a crack in the SEAM micrograph.

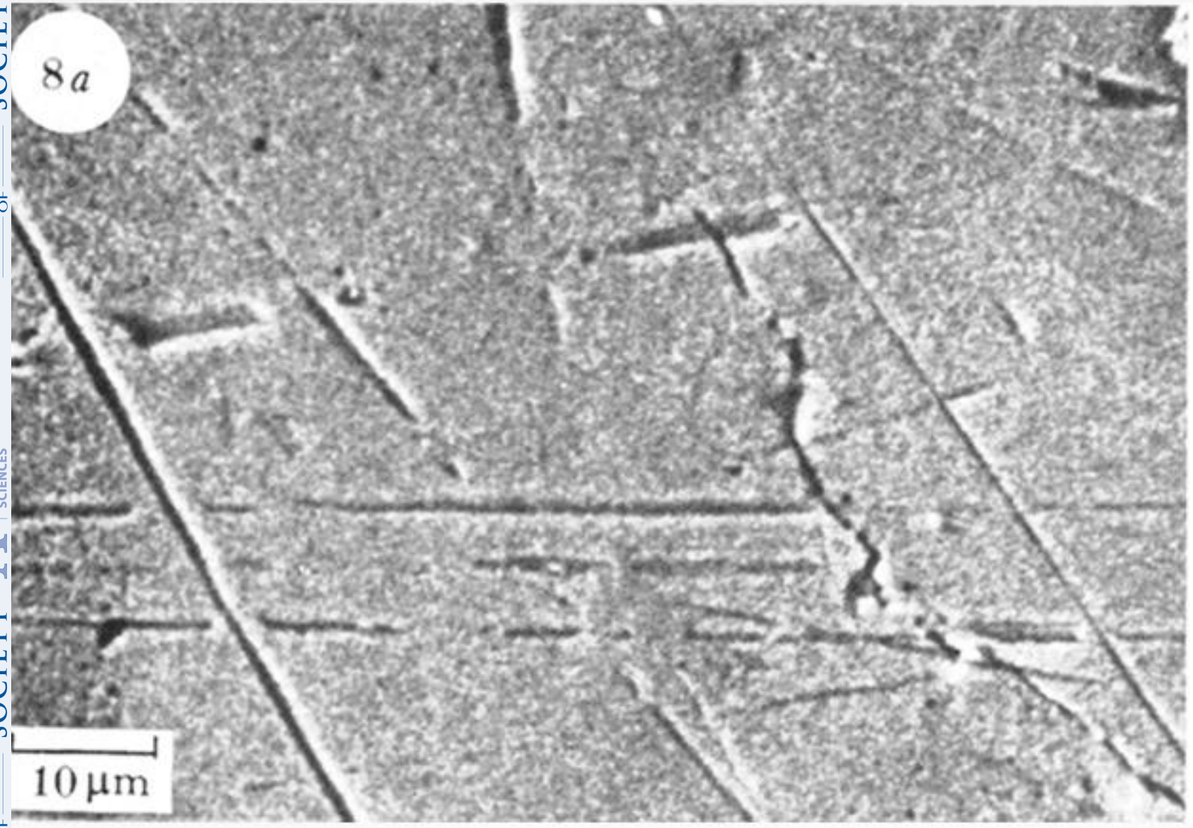

FIGURE 8. (*a*) SE image of a crack in an Fe–Ni–C alloy. (*b*) SEAM image reveals subsurface crack extending beyond visible crack tip, and also a second, completely subsurface crack.

FIGURE 9. (*a*) SE image of a crack in polystyrene and (*b*) SEAM image showing craze extending beyond the crack tip. The specimen was Cu-coated and imaged at 20 keV to avoid degradation.

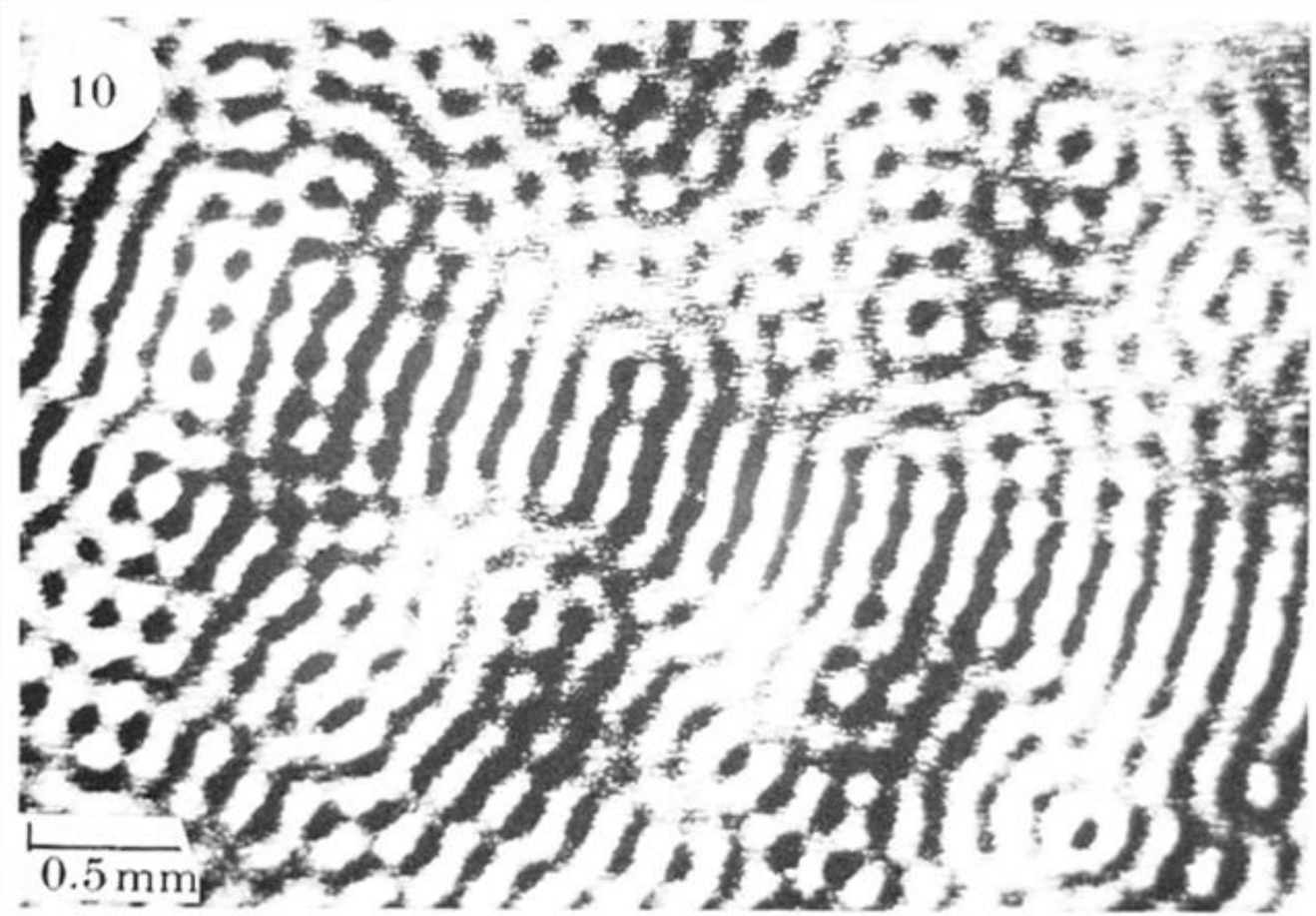

FIGURE 10. SEAM image showing vibrational pattern in a smooth, 16 μm thick Al foil at $f = 5.8$ MHz. The pattern has short wavelength (A) and long-wavelength (S) Lamb modes superimposed.

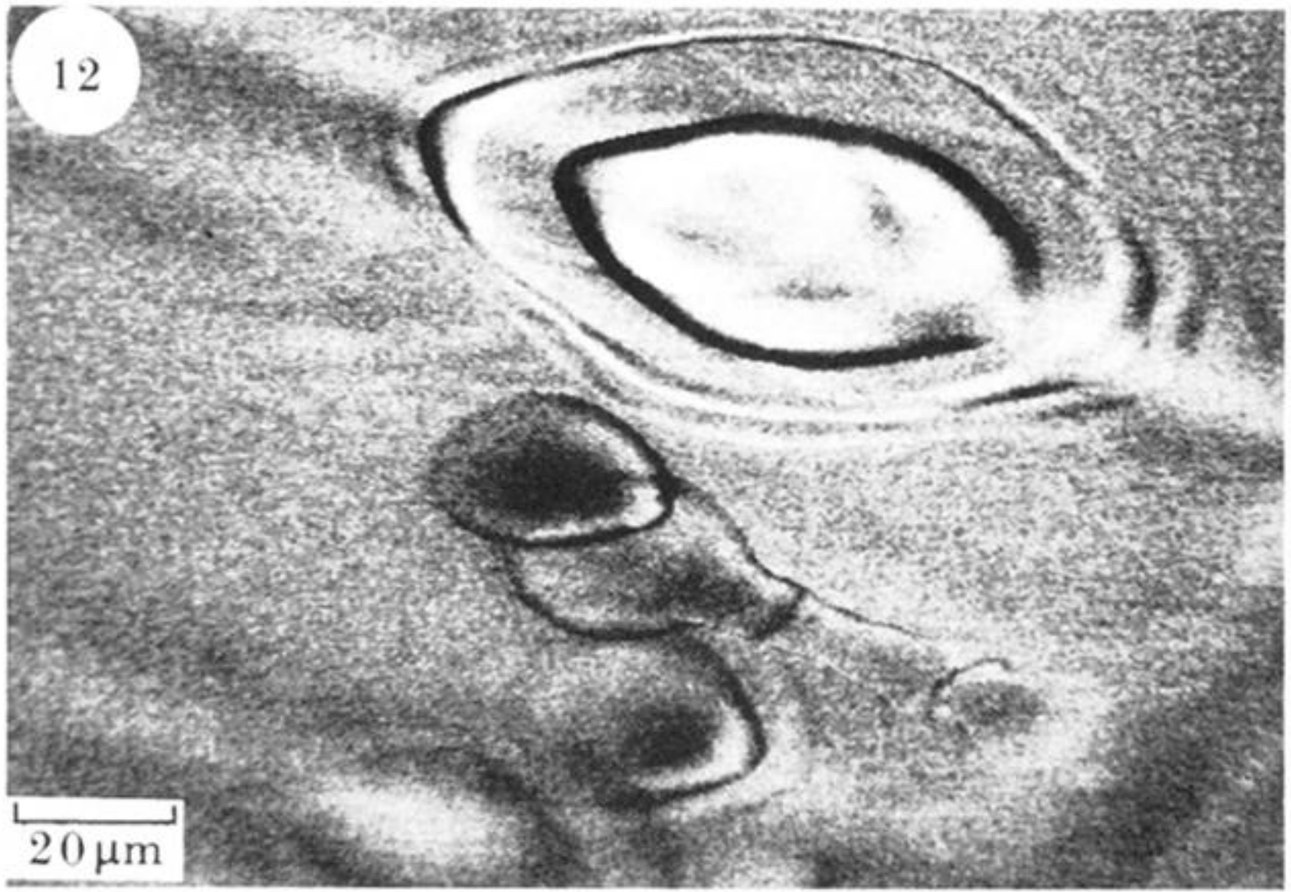

FIGURE 12. $2f = 220$ kHz nonlinear SEAM micrograph showing very fine ring features associated with martensite platelets in a Cu–Zn–Al alloy.

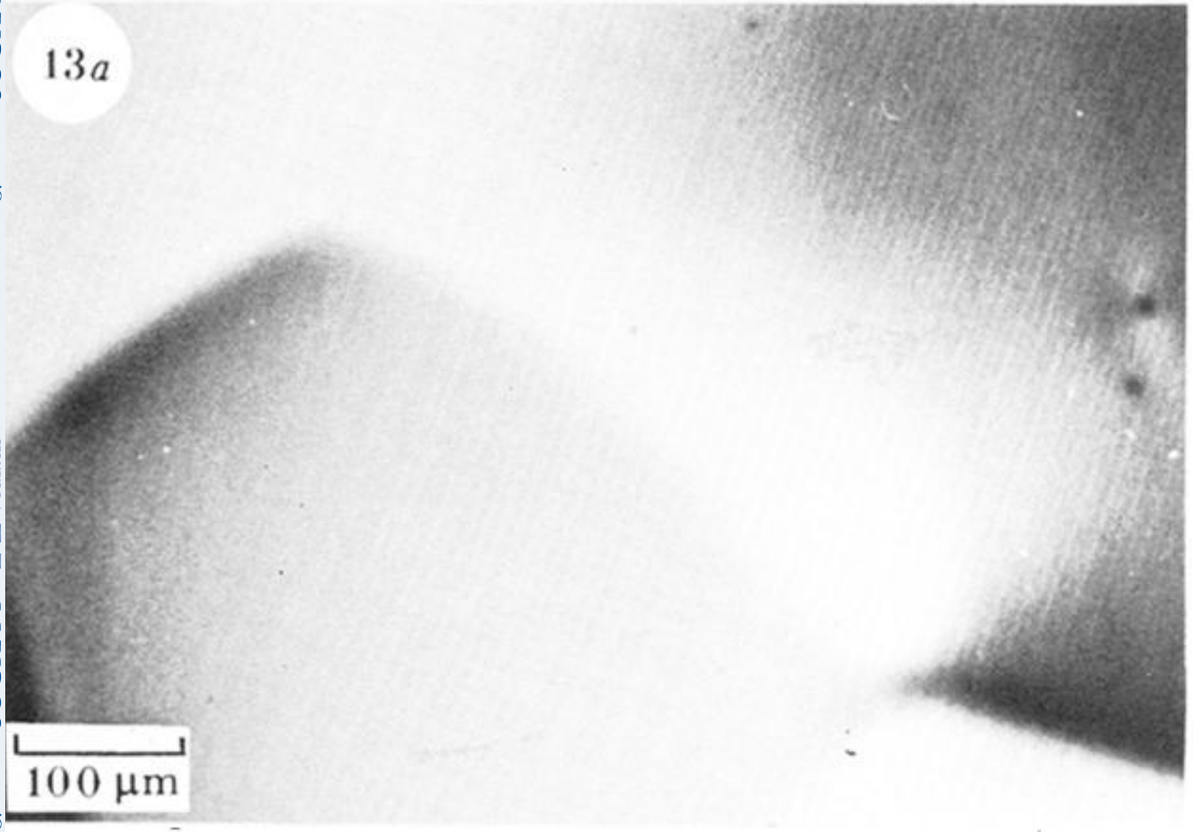

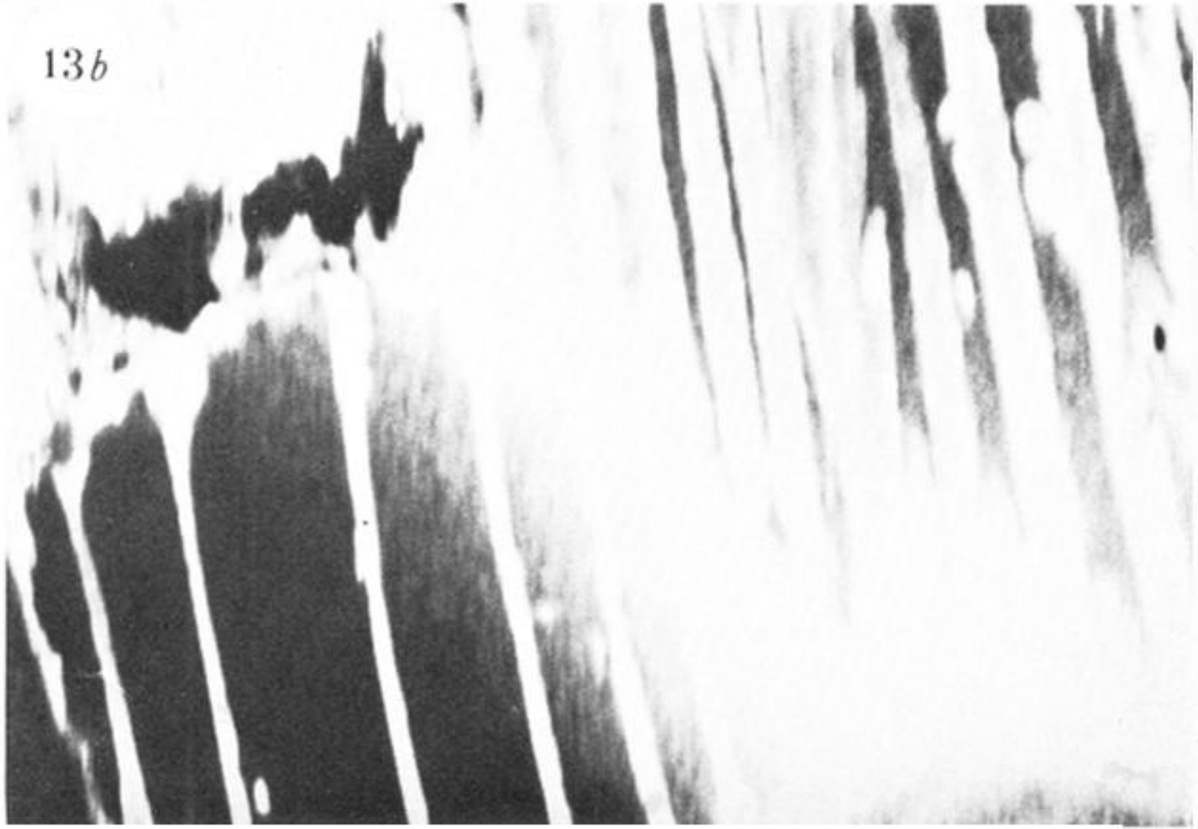

FIGURE 13. (*a*) Normal SEAM image showing only grain structure of a polished Fe–Si transformer sheet. (*b*) $2f = 253$ kHz nonlinear image of the same region reveals magnetic domain structures.